# Correcting Bidirectional Effects in Remote Sensing Reflectance from Coastal Waters

Yongzhen Fan[1], Zhenyi Lin [1], Wei Li[1], Knut Stamnes[1], Charles Gatebe[2,4], Rajesh Poudyal[3,4]

[1]LLLab, Stevens Institute of Technology, U.S.; [2]Universities Space Research Association, Columbia, Maryland; [3]Science Systems and Applications, Inc, Maryland; [4]NASA Goddard Space Flight Center, Greenbelt, Maryland

## Motivation

Understanding bidirectional effects including sunglint is important for GEO-CAPE for several reasons: (i) correct interpretation of ocean color data; (ii) comparing consistency of spectral radiance data derived from space observations with a single instrument for a variety of illumination and viewing conditions; (iii) merging data collected by different instruments operating simultaneously. We present a new neural network (NN) method to correct bidirectional effects in water-leaving radiance for both Case 1 and Case 2 waters. We also discuss a new BRDF and 2D sun-glint model that was validated by comparing simulated surface reflectances with Cloud Absorption Radiometer (CAR) data. Finally, we present an extension of our marine bio-optical model to the UV range that accounts for the seasonal dependence of the inherent optical properties (IOPs).

## The Neural Network Method

The bidirectional effect or the Bidirectional Reflectance Distribution Function (BRDF) has been studied extensively in the past few decades. The standard correction method developed by Morel et al. in 2002 (MAG02) is based on the Case 1 assumption making it unsuitable for application to coastal (Case 2) waters. We introduce a neural network (NN) method that can be applied to both Case 1 and Case 2 waters.

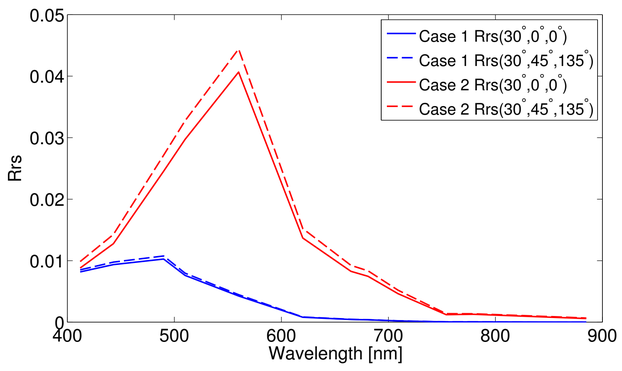


**Figure 1.** Simulated remote sensing reflectances.

Figure 1 shows 2 cases of simulated remote sensing reflectances. The difference between Case 1 and Case 2 waters is significant, but for each case, the difference is small between nadir-viewing remote sensing reflectance $R_{rs}(\lambda_i, \theta_0)$ and angle-dependent remote sensing reflectance $R_{rs}(\lambda_i, \theta_0, \theta, \Delta\phi)$. We found that a Radial Basis Function Neural Network (RBF-NN) can establish a direct connection between $R_{rs}(\lambda_i, \theta_0)$ and $R_{rs}(\lambda_i, \theta_0, \theta, \Delta\phi)$. We simulated 30,000 cases with different sun-sensor geometries and different water and atmospheric IOPs to include both Case 1 and Case 2 water conditions. Then we trained a neural network to derive the nadir-viewing $R_{rs}(\lambda_i, \theta_0)$ from the angle-dependent $R_{rs}(\lambda_i, \theta_0, \theta, \Delta\phi)$ directly.

## Summary and Further Work

- A new neural network (NN) method to correct bidirectional effects in remote sensing reflectance ($R_{rs}$) has been developed and validated by in-situ data (Fan et al. 2015).
- The new NN method shows a similar performance as the standard MAG02 algorithm in Case 1 water, but a significant improvement in Case 2 water.
- The bio-optical model was extended to the UV range and ia UV factor was introduced to account for seasonal dependence.
- A BRDF and 2D sunglint model (see another poster) was developed, and validation using Cloud Absorption Radiometer (CAR) BRDF data showed very good agreement.
- **Future work:** Several anisotropy correction tables will be provided for the ocean color community, including sunglint correction for both Case 1 and Case 2 water.

## References

- Y. Fan, W. Li, K. J. Voss and K. Stamnes, "A neural network method to correct bidirectional effect in water-leaving radiance," paper submitted to Appl. Opt. in July, 2015.
- Z. Lin, W. Li, C. Gatebe, R. Poudyal and K. Stamnes, "Simulation of the ocean glint reflectance and determination of the sea surface roughness," paper submitted to Remote Sen. Environ. in July, 2015.

## Marine Bio-Optical Model - CCRR

In the CCRR (Coast Color Round Robin) model, we assume that algal particles (CHL) and non-algal particles (MIN), in addition to detrital and dissolved organic matter (CDOM) are present in the water so that it can be used to represent both algal-dominated (Case 1) water and Case 2 coastal water. The IOPs are parameterized as:

$$a_{\mathrm{CHL}}(\lambda) = A(\lambda) \times \mathrm{CHL}^{E(\lambda)} \qquad b_{\mathrm{CHL}}(\lambda) = 0.407 \times \mathrm{CHL}^{0.795} \times (\lambda/660)^{\nu} - a_{\mathrm{CHL}}(\lambda)$$
$$a_{\mathrm{MIN}}(\lambda) = 0.031 \times \mathrm{MIN} \times \exp[-0.0123(\lambda - 443)] \qquad b_{\mathrm{MIN}}(\lambda) = 0.52 \times \mathrm{MIN} \times (\lambda/555)^{-0.3749} - a_{\mathrm{MIN}}(\lambda)$$
$$a_{\mathrm{CDOM}}(\lambda) = \mathrm{CDOM} \times \exp[-0.0176(\lambda - 443)]$$

where $A(\lambda)$ and $E(\lambda)$ are from the paper of Brichaud et al. (1998). $\nu = 0.5 \times (\log_{10}\mathrm{CHL} - 0.3)$, when $\mathrm{CHL} < 2.0$; and $\nu = 0$ when $\mathrm{CHL} > 2.0$. The model has been extended to UV range (300-400 nm) based on the papers by Morrison and Nelson (2004), and Vasilkov et al. (2005). In the UV range, the absorption coefficient of algal particles varies with season (absorption is higher in summer than than in winter). We introduced a UV factor that can be used to describe the seasonal dependence.

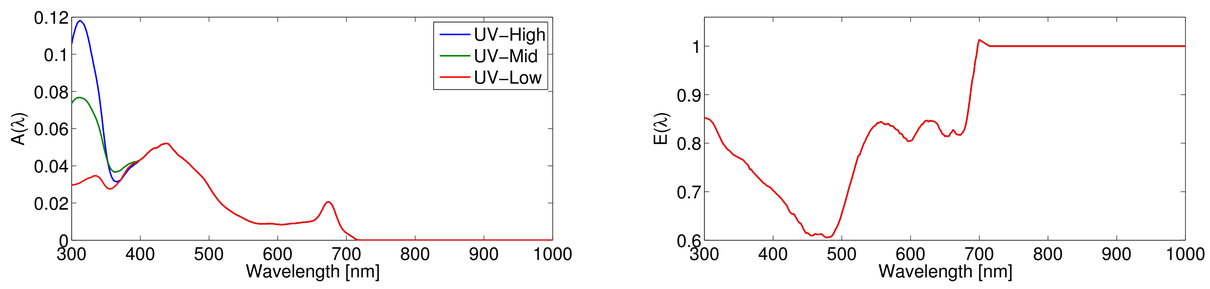


**Figure 2.** Extended $A(\lambda)$ and $E(\lambda)$ coefficient from 300nm to 1000nm.

## Anisotropy Correction: Synthetic Data Study and Validation of NN Method

We first analyzed a synthetic dataset to demonstrate the importance of the BRDF correction. We simulated 80,000 remote sensing reflectances for different sun-sensor geometries and water IOPs using AccuRT, which is a RTM for the coupled atmosphere-ocean system. The covariation and distribution of the marine parameters: CHL, CDOM and MIN are shown in Fig. 3. We computed the percentage error between the nadir viewing $R_{rs}(\theta_0)$ and the angle-dependent $R_{rs}(\theta_0, \theta, \Delta\phi)$, which can be used as an indicator of anisotropy. The error distribution is shown in Fig. 4. We found that for Case 1 water, the error incurred by the BRDF effect can go up to 25% with an average of 2.8%-5.1% for different wavelengths. For Case 2 water, the error can go up to 50%, and the average error increases to 9.7%-11%. We also found that the anisotropy in $R_{rs}$ depends strongly on sensor viewing angle, whereas the dependence on solar angle and relative azimuthal angle is relatively weak.

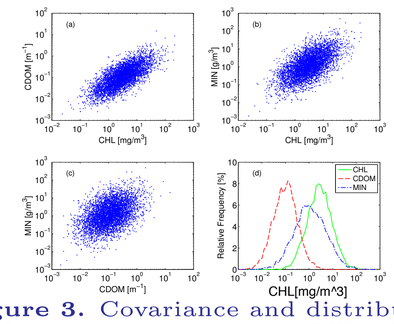


**Figure 3.** Covariance and distribution of the marine parameters: CHL, CDOM and MIN.

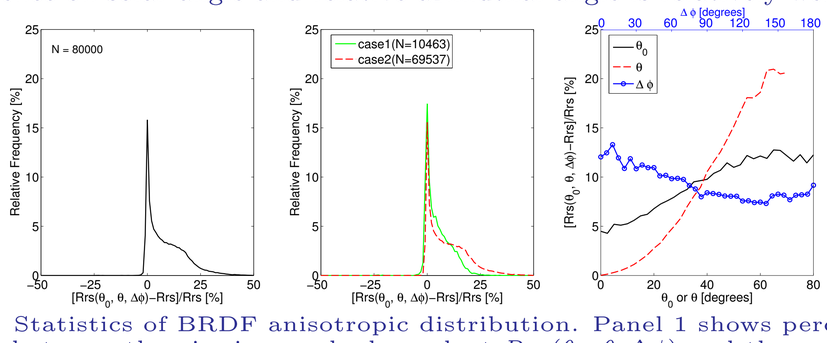


**Figure 4.** Statistics of BRDF anisotropic distribution. Panel 1 shows percentage difference between the viewing angle-dependent $R_{rs}(\theta_0, \theta, \Delta\phi)$ and the nadir viewing $R_{rs}(\theta_0)$ for 80,000 simulation data, panel 2 shows the distribution of the difference for Case 1 and Case 2 waters, and panel 3 shows the dependence on sun-sensor geometry.

We used the NuRADS field-measured BRDF data available in SeaBASS to validate our neural network BRDF correction method. Two datasets, BP09 and SORTIE2, were used for validation. BP09 was conducted in the Ligurian Sea in March, 2009 while an algal bloom was ongoing in the area, so the water was dominated by chlorophyll; SORTIE2 was conducted in January, 2008 near San Diego Bay, where the water is generally Case 2, with high concentrations of both chlorophyll and sediment particles. Figure 5 shows a comparison of the percentage error distribution of the BRDF derived from our NN method and the standard MAG02 method.

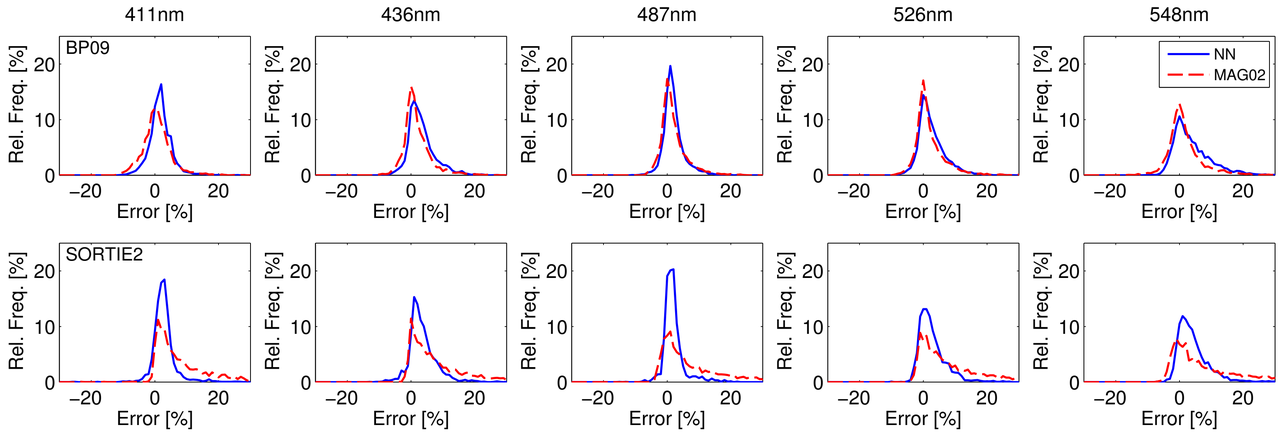


**Figure 5.** Comparison of the percentage error distribution of the BRDF derived from the NN and MAG02 algorithms.

## Validation of the BRDF and 2D Sun Glint Model with CAR Data

We developed a BRDF model and 2D sunglint model. Validation using surface reflectance data measured by the Cloud Absorption Radiometer (CAR) in July 10, 2001 over Chesapeake Bay shows good agreement (Fig. 6).

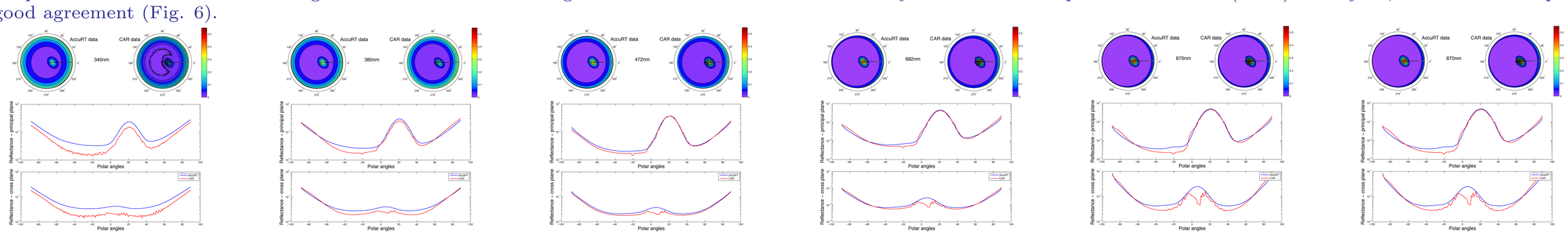


**Figure 6.** Comparison between our BRDF and 2D sun glint model simulated surface reflectances (blue) and CAR measured surface reflectances (red). From left to right, each column shows a comparison for 340 nm, 380 nm, 472 nm, 682 nm, 870 nm and 1036 nm, respectively. Within each column, the top panel shows a comparison of the entire surface reflectance, the middle panel shows a comparison of a line of data extracted from the principal plane, and the bottom panel shows the same as the middle panel but from 90° across the principal plane.